PCCP

COMMUNICATION

View Article Online
View Journal | View Issue

Cite this: *Phys. Chem. Chem. Phys.*, 2014, **16**, 13595

Received 22nd January 2014,
Accepted 27th February 2014

DOI: 10.1039/c4cp00341a

www.rsc.org/pccp

Electrocatalysis of hydrogen peroxide reactions on perovskite oxides: experiment *versus* kinetic modeling†

T. Poux,[a] A. Bonnefont,[b] A. Ryabova,[c] G. Kéranguéven,[a] G. A. Tsirlina[c] and E. R. Savinova*[a]

Hydrogen peroxide has been identified as a stable intermediate of the electrochemical oxygen reduction reaction on various electrodes including metal, metal oxide and carbon materials. In this article we study the hydrogen peroxide oxidation and reduction reactions in alkaline medium using a rotating disc electrode (RDE) method on oxides of the perovskite family ($LaCoO_3$, $LaMnO_3$ and $La_{0.8}Sr_{0.2}MnO_3$) which are considered as promising electrocatalytic materials for the cathode of liquid and solid alkaline fuel cells. The experimental findings, such as the higher activity of Mn-compared to that of Co-perovskites, the shape of RDE curves, and the influence of the H_2O_2 concentration, are rationalized with the help of a microkinetic model.

1. Introduction

Hydrogen peroxide has been identified as a stable intermediate of the electrochemical oxygen reduction reaction (ORR) on various electrodes including metal, metal oxide and carbon materials. In this article we study the hydrogen peroxide oxidation and reduction reactions (HPOR/HPRR) in alkaline medium on oxides of the perovskite family which are considered as promising electrocatalytic materials for the cathode of liquid and solid alkaline fuel cells. While several researchers studied the catalytic hydrogen peroxide decomposition kinetics on perovskite oxides, very few published results can be found for the study of the electrochemical HPOR/HPRR on perovskite oxides,[1–3] and these are unfortunately not sufficiently detailed.

Considering the value of pK_a of H_2O_2 (11.7[4]), in alkaline media it transforms into HO_2^-:

$$H_2O_2 + OH^- \leftrightarrows HO_2^- + H_2O \quad (I)$$

Four electrode reactions can theoretically occur in the presence of HO_2^-: HO_2^- reduction into OH^- (II), HO_2^- oxidation into O_2 (III), and the inverse reactions, OH^- oxidation into HO_2^- (−II) and O_2 reduction into HO_2^- (−III).

$$HO_2^- + 2e^- + H_2O \leftrightarrows 3OH^-,\ E^\circ = 1.71\ V_{RHE} \text{ at pH } 14 \quad (II)$$

$$HO_2^- + OH^- \leftrightarrows O_2 + H_2O + 2e^-,\ E^\circ = 0.77\ V_{RHE} \text{ at pH } 14 \quad (III)$$

Given the standard potential of the HO_2^-/OH^- couple, the OH^- oxidation into HO_2^- (step −II) is unlikely in the potential range of interest for a cathode of an alkaline fuel cell, and will be neglected in this work. Thus, the current–potential curve over a perovskite electrode in a H_2O_2 containing electrolyte is essentially determined by reactions II, III, and −III.

In this work, the HPOR and HPRR are studied using the rotating disc electrode (RDE) method on two oxides of the perovskite family, $LaCoO_3$ and $La_{0.8}Sr_{0.2}MnO_3$, which demonstrated distinct behavior in the ORR (see our recent work in ref. 5), as well as on $LaMnO_3$. The activity of the oxide materials is compared with that of Pt/C, a reference material in fuel cell electrocatalysis, and with carbon. The latter is an essential component of transition metal oxide-based cathodes improving their electronic conductivity, and thus the degree of the catalyst utilization. To better understand the mechanism of the HPOR and HPRR, and the ORR, on perovskite oxides, a kinetic model is proposed, and the experimental RDE curves are compared with the simulated ones. The study of the influence of the H_2O_2 concentration on the HPOR and HPRR allows one to shed light on the reaction kinetics and helps to validate the model assumptions.

[a] *Institut de Chimie et Procédés pour l'Energie, l'Environnement et la Santé, UMR 7515 CNRS-University of Strasbourg, 25 rue Becquerel, 67087 Strasbourg Cedex, France. E-mail: Elena.Savinova@unistra.fr; Fax: +33(0)3 68 85 27 61; Tel: +33(0)3 68 85 27 39*

[b] *Institut de Chimie de Strasbourg, UMR 7177 CNRS-University of Strasbourg, 4 rue Blaise Pascal, 67070 Strasbourg, France*

[c] *Faculty of Chemistry, Lomonosov Moscow State University, 119991 Leninskie Gory, Moscow, Russia*

† Electronic supplementary information (ESI) available. See DOI: 10.1039/c4cp00341a

2. Experimental

$LaCoO_3$, $LaMnO_3$ and $La_{0.8}Sr_{0.2}MnO_3$ were synthesized at the Moscow State University using polyacrylamide gel by a soft chemistry method, which offers materials with higher surface areas than conventional high temperature approaches. For the synthesis procedure the reader is referred to ref. 5. Specific surface areas of $LaCoO_3$, $LaMnO_3$ and $La_{0.8}Sr_{0.2}MnO_3$ measured by BET were 10, 14 and 17 $m^2\ g^{-1}$, respectively. Oxides were mixed with carbon and deposited on a glassy carbon RDE (0.07 cm^2 geometric area, Autolab) in the form of a thin layer.[5] Carbon of the Sibunit family with a BET surface area of 65.7 $m^2\ g^{-1}$ was chosen due to its high purity and high electron conductivity.[6] In order to improve the adhesion of the perovskite and carbon particles onto the GC support, an alkaline ionomer (AS-4 from Tokuyama Company) was deposited on top of the dry catalyst layer to form a thin film (the ionomer loading was 2.4 μg cm^{-2}). For further details on the electrode preparation the reader is referred to ref. 5. For all oxide/carbon loadings utilized in this work the catalytic layer thickness was smaller than the diffusion layer thickness.

Pt/C electrodes were prepared by drop-casting a suspension containing Pt/C (40 wt% Pt on carbon black, Alfa Aesar) to obtain 20 μg cm^{-2} Pt loading. The roughness factor of Pt on the electrode estimated using the coulometry of the hydrogen underpotential deposition was equal to 6.

Electrochemical measurements were performed at 25 °C in a three electrode cell whose parts in contact with the electrolyte were made out of Teflon. The electrolyte was 1 M NaOH prepared from extra pure NaOH solution (50 wt% solution in water, Acros Organics) and ultrapure water (Purelab: 18.2 MΩ cm, <3 ppb TOC). The counter electrode was a platinum wire and the reference electrode was a Hg/HgO/1 M NaOH electrode (IJ Cambria Scientific). In what follows the electrode potentials are given in the RHE (reversible hydrogen electrode) scale. RDE curves were IR-corrected by using the value of the electrolyte resistance (15 Ohm) determined from the high frequency part of the electrochemical impedance spectra (measured in the 1 Hz to 100 kHz range). Electrochemical measurements were performed using an Autolab potentiostat with an analog scan generator at a scan rate of 10 mV s^{-1}. H_2O_2 solutions were prepared from 30 wt% solution in water (SupraPur, Merck) titrated with standardized $KMnO_4$.

3. Results and discussion

Fig. 1a shows positive scans of RDE voltammograms in N_2-purged 1 M NaOH containing 0.84 mM H_2O_2 for $LaCoO_3$/carbon, $LaMnO_3$/carbon and $La_{0.8}Sr_{0.2}MnO_3$/carbon composite electrodes, as well as for Pt/C and Sibunit carbon. Such H_2O_2 concentration was chosen since it corresponds to the O_2 concentration in the O_2 saturated electrolyte. For Pt/C in agreement with the literature data[7–10] the voltammogram is reversible, suggesting fast hydrogen peroxide oxidation and reduction reactions, and the anodic and cathodic current plateaus correspond to the diffusion limited HPOR and HPRR,

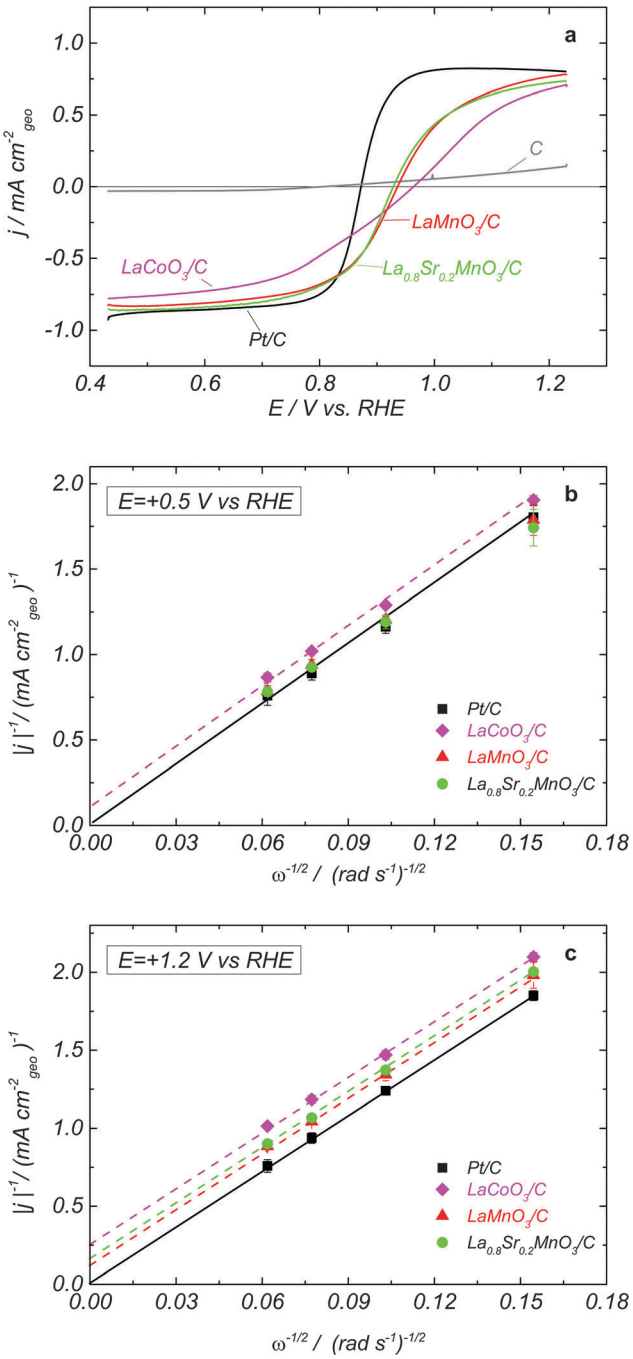

Fig. 1 (a) Positive scans of the RDE voltammograms in N_2-purged 1 M NaOH + 0.84 mM H_2O_2 at 900 rpm and 10 mV s^{-1} and corresponding Levich–Koutecky plots at +0.5 V_{RHE} (b) and at +1.2 V_{RHE} (c) for GC-supported thin films of $LaCoO_3$ + C (magenta), $LaMnO_3$ + C (red), $La_{0.8}Sr_{0.2}MnO_3$ + C (green), C (grey) and Pt/C (black). Catalyst loadings are 91 μg cm^{-2} perovskite + 37 μg cm^{-2} carbon for oxide electrodes, 37 μg cm^{-2} for carbon electrodes, and 50 μg cm^{-2} for Pt/C electrodes. Currents are normalized to the electrode geometric area and corrected to the background currents measured in a N_2 atmosphere. Error bars in panels (b) and (c) represent standard deviations from at least two independent repeated measurements.

as confirmed by the Levich–Koutecky (LK) plots shown in Fig. 1b and c. For Sibunit carbon, the voltammogram is strongly irreversible, pointing to a very slow HPOR and an even slower

HPRR (Fig. 1, grey curve). For oxide/carbon composites, both the anodic and the cathodic waves have smaller slopes compared to Pt, pointing out at slower electrocatalysis of hydrogen peroxide reactions on studied perovskite oxides. Furthermore, the mixed potential values, where the sum of currents of all electrode reactions (reactions II/−II and III/−III) is equal to zero, for perovskite oxides are shifted positive compared to those of Pt/C, suggesting a slower HO_2^- oxidation, notably for $LaCoO_3$. In the absence of carbon, perovskite oxides show slower hydrogen peroxide oxidation/reduction kinetics (Fig. S1, ESI†). However, contrary to what has recently been demonstrated for the ORR on oxides of the perovskite family, where carbon plays a dual role, (i) improving the interparticle contact, and also (ii) participating in the ORR electrocatalysis, the enhancement of the rates of HPOR and HPRR is predominantly due to the first factor (improvement of the electronic conductivity of the catalytic layer). This is due to the low catalytic activity of carbon in HO_2^- reactions (*cf.* Fig. 1a, grey curve). Note also that for $LaMnO_3$ the effect of addition of carbon on the RDE curves is stronger compared to that for the $La_{0.8}Sr_{0.2}MnO_3$. This can be attributed to a higher intrinsic electron conductivity of the doped compared for the undoped Mn-based perovskite (for further details see ESI†).

The Mn-based $LaMnO_3$ and $La_{0.8}Sr_{0.2}MnO_3$ perovskites display close mixed potentials (similar trends can be found in the literature for $La_{1-x}Sr_xMnO_3$[1]), and very similar activities for HO_2^- reduction/oxidation, once sufficient amount of carbon is present in the catalytic layer (Fig. 1a). Moreover, their HO_2^- reduction and oxidation currents approach the diffusion plateau reached by the Pt/C electrode at low and high potentials, respectively (note however that at 1.2 V the intercepts of the LK plots are non-zero). This suggests that on Mn perovskite oxides at high overpotentials the HPOR and HPRR are diffusion-limited. For $LaCoO_3$ electrodes, the currents do not reach the plateaus of Pt/C, due to a slower HO_2^- reduction and oxidation kinetics. The comparison of the current slope near the mixed potential for various perovskites (Fig. 1a) confirms that $LaCoO_3$ is less catalytically active in HO_2^- reactions than either $LaMnO_3$ or $La_{0.8}Sr_{0.2}MnO_3$. Since the mixed potential of $LaCoO_3$ is positively shifted compared to that of Mn perovskite oxides, we conclude that the HPOR is slower than the HPRR on the cobalt perovskite. The cathodic branch of the RDE voltammograms for $LaCoO_3$ shows two slopes (Fig. 1a) suggesting that at least two steps are involved in the HO_2^- reduction reaction. In what follows this hypothesis will be corroborated with the help of a mathematical model.

The influence of the H_2O_2 concentration on the HPOR and HPRR kinetics is shown in Fig. 2a for $La_{0.8}Sr_{0.2}MnO_3$. While the absolute values of the limiting anodic and cathodic currents increase proportionally to the H_2O_2 concentration, the mixed

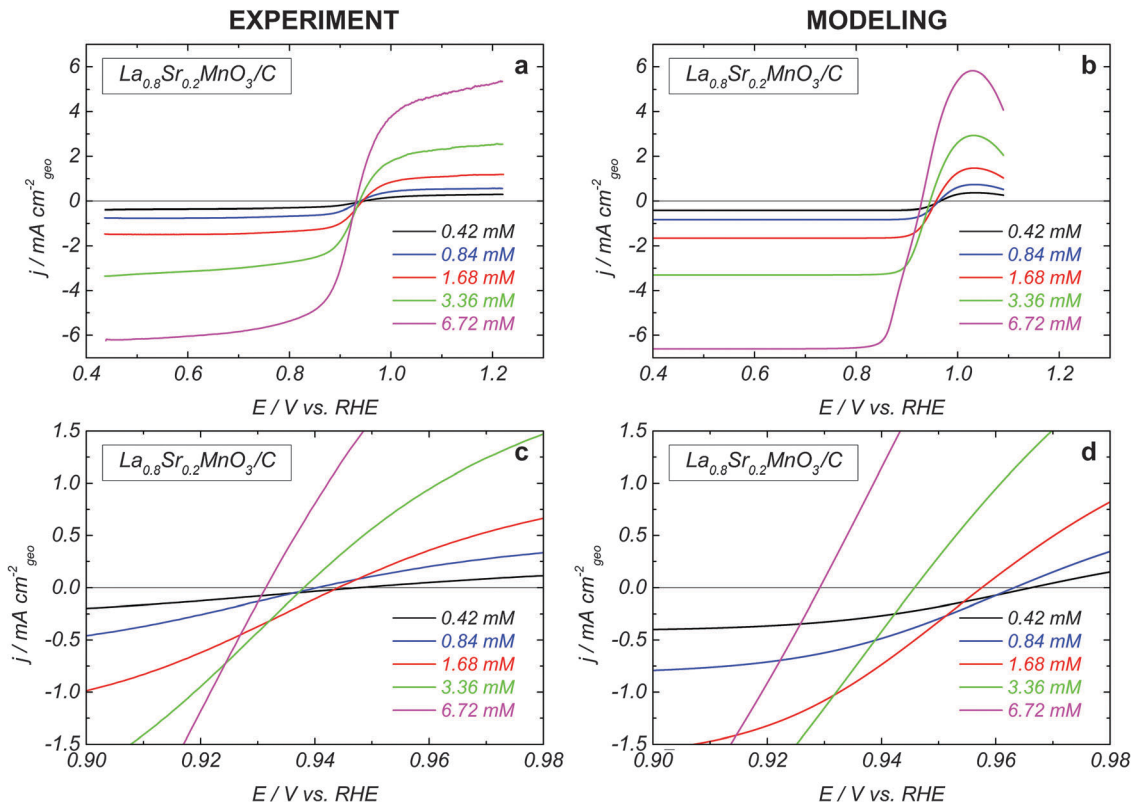

Fig. 2 (a) Experimental positive scans of the RDE voltammograms in N_2-purged solutions of 1 M NaOH and various H_2O_2 concentrations at 900 rpm and 10 mV s^{-1} for GC-supported thin films of $La_{0.8}Sr_{0.2}MnO_3$ (91 μg cm^{-2}) + carbon (74 μg cm^{-2}). Currents are normalized to the geometric area of the electrode and corrected to the background currents measured in a N_2 atmosphere. (b) Simulated RDE voltammograms. (c) and (d) show close-ups for experimental (c) and simulated (d) voltammograms. For details see the text.

potential is displaced towards the negative values (see close-up in Fig. 2c). The same behavior was observed for $LaCoO_3$ (not shown). This indicates that the perovskite oxide-catalyzed HO_2^- reduction and the HO_2^- oxidation reactions have different concentration dependences.

In order to better understand the experimental findings, a microkinetic model was developed. Note that the mathematical model serves to understand the influence of the experimental parameters (potential and concentration), the differences between Mn and Co perovskites, and to verify the consistency of the proposed reaction mechanism with the experimental data, rather than to accurately determine the values of the rate constants. The elementary steps for the HO_2^- and O_2 adsorption and reaction on perovskite oxides were inspired by the experimental studies of Goodenough[11] and Suntivich *et al.*[12] and the density functional theory (DFT) calculations of Wang and Cheng,[13] and adapted in order to reproduce the experimental findings of this work.

Since the oxide surface in an alkaline electrolyte is supposed to be covered by OH_{ad},[11,14] displacement of OH_{ad} by either O_2 or HO_2^- is likely to be the first step in the electrocatalysis of O_2[11] and H_2O_2 reactions.

$$HO_2^- + OH_{ad} \rightleftarrows HO_{2,ad} + OH^- \quad (1)$$

The adsorbed $HO_{2,ad}$ may be oxidized into oxygen in the reverse step of reaction (2):

$$O_{2,ad} + H_2O + e^- \leftrightarrows HO_{2,ad} + OH^- \quad (2)$$

The adsorbed oxygen molecule resulting from the backward step of reaction (2) may desorb in the reverse step of reaction (3). In agreement with the literature,[11,13] we suppose that upon adsorption oxygen molecules displace hydroxo species on the oxide surface:

$$O_2 + OH_{ad} + e^- \leftrightarrows O_{2,ad} + OH^- \quad (3)$$

The adsorbed $HO_{2,ad}$ can also undergo reduction. To account for the negative shift of the mixed potential with the increase of the H_2O_2 concentration, the HPOR and the HPRR must have different concentration dependence. In order to reproduce this, we assume that the $HO_{2,ad}$ reduction occurs in a sequence of chemical and electrochemical steps:

$$HO_{2,ad} + OH_{ad} \rightleftarrows 2O_{ad} + H_2O \quad (4)$$

$$O_{ad} + H_2O + e^- \leftrightarrows OH_{ad} + OH^- \quad (5)$$

Note that steps (1)–(5) also account for the catalytic decomposition of H_2O_2 occurring under open circuit conditions.

Considering both the experimental and the literature data we suppose that O_{ad} species are adsorbed on transition metal (B) cations in the high oxidation state $B^{(m+1)+}$ (B=O), while OH_{ad} species – on B-cations in the low oxidation state B^{m+} (B–OH). According to the DFT calculations of Wang and Cheng,[13] these intermediates (OH_{ad} and O_{ad}) are indeed strongly adsorbed on the surface of perovskite oxides.

Assuming Langmuir-type adsorption isotherms and Butler–Volmer type of the electrochemical kinetics, the reaction rates may be expressed as follows:

$$v_1 = k_1 c^S_{HO_2^-}\left(1 - \theta_{O_2} - \theta_{HO_2} - \theta_O\right) - k_{-1}\theta_{HO_2} \quad (6)$$

$$v_2 = k_2\theta_{O_2}\exp\left(\frac{-(1-\alpha)FE}{RT}\right) - k_{-2}\theta_{HO_2}\exp\left(\frac{\alpha FE}{RT}\right) \quad (7)$$

$$v_3 = k_3 c^S_{O_2}\left(1 - \theta_{O_2} - \theta_{HO_2} - \theta_O\right)\exp\left(\frac{-(1-\alpha)FE}{RT}\right) - k_{-3}\theta_{O_2}\exp\left(\frac{\alpha FE}{RT}\right) \quad (8)$$

$$v_4 = k_4\theta_{HO_2}(1 - \theta_{O_2} - \theta_{HO_2} - \theta_O) \quad (9)$$

$$v_5 = k_5\theta_O\exp\left(\frac{-(1-\alpha)FE}{RT}\right) - k_{-5}(1 - \theta_{O_2} - \theta_{HO_2} - \theta_O)\exp\left(\frac{\alpha FE}{RT}\right) \quad (10)$$

where $c^S_{HO_2^-}$, $c^S_{O_2^-}$ are the concentrations in front of the electrode at $x = 0$ (x is the distance along the normal to the electrode surface) and θ_{HO_2}, θ_{O_2}, θ_O the coverages of adsorbed intermediates, with $\theta_{OH} = 1 - \theta_{O_2} - \theta_{HO_2} - \theta_O$. α is the charge transfer coefficient, $F = 96\,486$ C mol^{-1} is the Faraday constant, $R = 8.314$ J K^{-1} mol^{-1} the ideal gas constant and $T = 300$ K the absolute temperature.

Under stationary conditions, this reaction scheme can be cast into a set of equations determining the concentrations of HO_2^- and O_2 in front of the electrode surface, and the coverages of adsorbed intermediates, $HO_{2,ad}^-$, $O_{2,ad}$, O_{ad}, and OH_{ad} on perovskite sites:

$$D_{O_2}\left(\frac{\partial c_{O_2}}{\partial x}\right) = -\frac{D_{O_2}c^S_{O_2}}{\delta_{O_2}} = \Gamma_{geo}v_3 \quad (11)$$

$$D_{HO_2^-}\left(\frac{\partial c_{HO_2^-}}{\partial x}\right) = \frac{D_{HO_2^-}\left(c^b_{HO_2^-} - c^S_{HO_2^-}\right)}{\delta_{HO_2^-}} = \Gamma_{geo}v_1 \quad (12)$$

$$\frac{d\theta_{O_2}}{dt} = v_3 - v_2 = 0 \quad (13)$$

$$\frac{d\theta_{HO_2}}{dt} = v_1 + v_2 - v_4 = 0 \quad (14)$$

$$\frac{d\theta_O}{dt} = 2v_4 - v_5 = 0 \quad (15)$$

where δ_i is the diffusion layer thickness, $c^b_{HO_2^-}$, the concentration of HO_2^- in the bulk of the electrolyte, and Γ_{geo} stands for the number of active sites per geometric area of the electrode. The overall current density is given by eqn (16).

$$j = -F\Gamma_{geo}(v_2 + v_3 + v_5) \quad (16)$$

A linear concentration profile for O_2 and HO_2^- is assumed in front of the electrode surface. The electrode thickness is assumed to be sufficiently small to keep this linear

Table 1 Rate constants used in the mathematical model to simulate the experimental curves of $LaCoO_3$ and $La_{0.8}Sr_{0.2}MnO_3$ electrodes

Rate constant	Units	Value	
		$LaCoO_3$	$La_{0.8}Sr_{0.2}MnO_3$
k_1	$cm^3\ mol^{-1}\ s^{-1}$	5×10^7	5×10^7
k_{-1}	s^{-1}	50	50
k_2	s^{-1}	5.1×10^8	5.1×10^9
k_{-2}	s^{-1}	4.9×10^{-8}	4.9×10^{-7}
k_3	$cm^3\ mol^{-1}\ s^{-1}$	1.6×10^{11}	1.6×10^{12}
k_{-3}	s^{-1}	1.6×10^{-8}	1.6×10^{-7}
k_4	s^{-1}	40	40
k_5	s^{-1}	6×10^7	1.2×10^8
k_{-5}	s^{-1}	2.9×10^{-9}	5.8×10^{-9}

concentration profile. The diffusion coefficients of O_2 and HO_2^- in 1 M NaOH were determined as $D_{O_2} = 1.5 \times 10^{-5}\ cm^2\ s^{-1}$ and $D_{HO_2^-} = 0.8 \times 10^{-5}\ cm^2\ s^{-1}$, respectively, from the corresponding diffusion limited current plateaus for Pt/C electrodes. Thus, the diffusion layer thickness at 900 rpm is $\delta_{O_2} = 19\ \mu m$ for O_2 and $\delta_{HO_2^-} = 15\ \mu m$ for HO_2^-.

Assuming that B cations act as active sites, the number of active sites per geometric surface area Γ_{geo} was calculated from the catalyst loading and the number of B sites per unit of the real surface area, which was estimated from the crystalline structure of perovskite oxides as $4.14 \times 10^{-10}\ mol\ cm^{-2}{}_{oxide}$. The values of the reaction rate constants were adjusted in order to reproduce the main features of the experimental RDE voltammograms for HPOR and HPRR, as well as for the ORR,[5] and are given in Table 1. Symmetry factors were all considered to be equal to 0.5, which is realistic for low and moderate overvoltages considered in this work. The adsorption–desorption rates of HO_2^- on perovskite sites directly depend on the values of k_1 and k_{-1} which have to be considered sufficiently high for adsorption and low for desorption to account for the significant activity of perovskites in the HPRR. k_2 and k_3 were adjusted to reproduce both the onset potential and the Tafel slopes for the ORR on perovskite oxides,[5] while the rate constants of the reverse reactions k_{-2}, k_{-3} were chosen to account for the standard potential of the O_2/HO_2^- at 0.77 V *vs.* RHE. Finally, the values of the mixed potential for the HPRR/HPOR and the potential of the $B^{(m+1)+}/B^{(m)+}$ redox peaks (see CVs in ref. 5) were used to adjust the values of k_4, k_5 and k_{-5}.

Fig. 3 shows simulated RDE voltammograms for $LaCoO_3$ and $La_{0.8}Sr_{0.2}MnO_3$ oxides. The rate constants are listed in Table 1, and an almost reversible voltammogram is obtained for $La_{0.8}Sr_{0.2}MnO_3$ (Fig. 3b). By choosing smaller rate constants for steps 2, 3 and 5, we are able to reproduce a slower HPOR on $LaCoO_3$ (*cf.* Fig. 3a and b) and a positive shift of the mixed potential compared to $La_{0.8}Sr_{0.2}MnO_3$. Furthermore, the assumption of the $HO_{2,ad}$ reduction as a sequence of two elementary steps allows us to reproduce the observed change of the slope of the HPRR on $LaCoO_3$. Fig. 3 also shows the splitting of the RDE voltammograms into a sum of three main contributions for two HO_2^- concentrations. The anodic branch corresponds to the HO_2^- oxidation into O_2 (step III), while the cathodic branch consists of two contributions: the HO_2^- reduction into OH^- (step II) and the O_2 reduction (this oxygen is formed in the anodic branch) into HO_2^- (step −III). One may note that the differences between $LaCoO_3$ and $La_{0.8}Sr_{0.2}MnO_3$ are partly due to the lower ORR activity of $LaCoO_3$ (*cf.* blue curves in Fig. 3a and b). For experimental ORR data on $LaCoO_3$ and $La_{0.8}Sr_{0.2}MnO_3$ the reader is referred to our earlier publication.[5]

The influence of the H_2O_2 concentration can be traced from simulated voltammograms shown in Fig. 2b, d and 3b. Increasing the concentration directly affects the reaction rate of the adsorption–desorption of HO_2 (reaction (1)) and therefore the site coverage by $HO_{2,ad}$ species (θ_{HO_2}). In the anodic direction, an increase of θ_{HO_2} causes an increase in the rate (step −2) of formation of $O_{2,ad}$ from $HO_{2,ad}$ (*cf.* dashed over solid green lines in Fig. 3b). On the other hand, in the cathodic branch, an increase of the HO_2^- concentration does not lead to a strong acceleration of reaction (4), since its rate depends on both θ_{HO_2} and $\theta_{OH} = (1 - \theta_{O_2} - \theta_{HO_2} - \theta_O)$ (*cf.* dashed over solid magenta lines in Fig. 3b). A stronger concentration dependence of the HO_2^- oxidation compared to the reduction counterpart, and the potential dependence of the former result in the negative shift of the mixed potential with the HO_2^- concentration (Fig. 3b, black curves, and Fig. 2b and d).

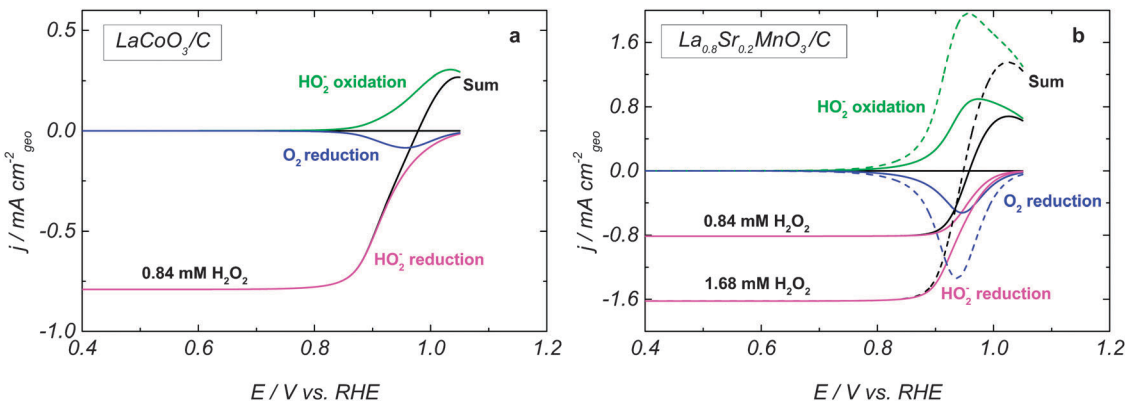

Fig. 3 Simulated RDE voltammograms for (a) $LaCoO_3$ and (b) $La_{0.8}Sr_{0.2}MnO_3$ in 0.84 mM H_2O_2 (solid lines) and 1.68 mM H_2O_2 (dashed lines) at 900 rpm. The number of sites per geometric surface area is $3.8 \times 10^{-9}\ mol\ cm^{-2}{}_{geo}$ for $LaCoO_3$ and $6.4 \times 10^{-9}\ mol\ cm^{-2}{}_{geo}$ for $La_{0.8}Sr_{0.2}MnO_3$. Color codes for the individual contributions: HO_2^- reduction (magenta), O_2 reduction (blue), HO_2^- oxidation (green), and total current obtained by the addition of the previously mentioned contributions (black). Currents are calculated per geometric area of the electrode.

The deconvolution of the whole current into individual contributions shows that the kinetic currents of the HO_2^- reduction/oxidation cannot be directly obtained from the total currents, contrary to what has been suggested in the literature.[15]

The main difference between the simulated and the experimental curves is the decrease of the HO_2^- oxidation current at high potentials for the former. It is caused by the oxidation of B^{m+} cations (which in our model are required for the adsorption of HO_2^-) into $B^{(m+1)+}$ cations at high potentials. Various possible explanations may be offered in order to account for the absence of such a current drop in the experiment, among these (i) surface heterogeneity resulting in a wide potential distribution of the $B^{m+}/B^{(m+1)+}$ red-ox transitions, (ii) adsorption of HO_2^- on $B^{(m+1)+}$ sites as well, (iii) carbon contribution to the HPOR at high electrode potentials (see grey curve in Fig. 1).

4. Conclusions

In this work, it is demonstrated that the $LaCoO_3$, $LaMnO_3$ and $La_{0.8}Sr_{0.2}MnO_3$ perovskite oxides, when mixed with carbon, show significant activity towards hydrogen peroxide reduction/oxidation reactions, with $LaCoO_3$ being less active than Mn perovskites. The kinetics of the hydrogen peroxide oxidation/reduction reactions on perovskite oxides can be reasonably described with a simple kinetic model. Modeling helps to rationalize the observed differences between Co and Mn perovskite oxides in H_2O_2 electrocatalysis, which are largely due to the lower electrocatalytic activity of Co perovskite for the H_2O_2 oxidation and O_2 reduction. Furthermore, it allows one to explain the H_2O_2 concentration dependence (including the displacement of the mixed potential with the concentration) by the multistep mechanism of the hydrogen peroxide reduction. The conclusions obtained have far-reaching consequences for the understanding of the ORR electrocatalysis on oxides of the perovskite family and will be further corroborated in our forthcoming publication.

Acknowledgements

The authors thank E.V. Antipov, S.Ya. Istomin and F.S. Napolskiy of the Moscow State University (Russia) for the synthesis and characterization of perovskite materials and for valuable discussions, P. Simonov of the Boreskov Institute of Catalysis (Novosibirsk, Russia) for supplying Sibunit Carbon, and Tokuyama Company for supplying alkaline ionomer. Financial support from CNRS (France), Region Alsace, Russian Foundation for Basic Research, and the French Ministry for the PhD scholarship of T.P. is gratefully appreciated.

References

1 G. Wang, Y. Bao, Y. Tian, J. Xia and D. Cao, Electrocatalytic activity of perovskite $La_{1-x}Sr_xMnO_3$ towards hydrogen peroxide reduction in alkaline medium, *J. Power Sources*, 2010, **195**, 6463–6467.

2 S. Zhuang, S. Liu, C. Huang, F. Tu, J. Zhang and Y. Li, Electrocatalytic activity of nanoporous perovskite $La_{1-x}Ca_xCoO_3$ towards hydrogen peroxide reduction in alkaline medium, *Int. J. Electrochem. Sci.*, 2012, **7**, 338–344.

3 Y. Matsumoto, H. Yoneyama and H. Tamura, The mechanism of oxygen reduction at a $LaNiO_3$ electrode, *Bull. Chem. Soc. Jpn.*, 1978, **51**, 1927–1930.

4 D. Dobos, *Electrochemical Data*, Akademiai Kiado, Budapesht, 1978.

5 T. Poux, F. S. Napolskiy, T. Dintzer, G. Kéranguéven, S. Ya. Istomin, G. A. Tsirlina, E. V. Antipov and E. R. Savinova, Dual role of carbon in the catalytic layers of perovskite/carbon composites for the electrocatalytic oxygen reduction reaction, *Catal. Today*, 2012, **189**, 83–92.

6 Y. I. Yermakov, V. F. Surovikin, G. V. Plaksin, V. A. Semikolenov, V. A. Likholobov, L. V. Chuvilin and S. V. Bogdanov, New carbon material as support for catalysts, *React. Kinet. Catal. Lett.*, 1987, **33**, 435–440.

7 V. G. Prabhu, L. R. Zarapkar and R. G. Dhaneshwar, Electrochemical studies of hydrogen peroxide at a platinum disc electrode, *Electrochim. Acta*, 1981, **26**, 725–729.

8 I. Katsounaros, W. B. Schneider, J. C. Meier, U. Benedikt, P. U. Biedermann, A. A. Auer and J. J. Mayrhofer, Hydrogen peroxide electrochemistry on platinum: towards understanding the oxygen reduction reaction mechanism, *Phys. Chem. Chem. Phys.*, 2012, **14**, 7384–7391.

9 A. M. Gomez-Marin, K. J. P. Schouten, M. T. M. Koper and J. M. Feliu, Interaction of hydrogen peroxide with a Pt(111) electrode, *Electrochem. Commun.*, 2012, **22**, 153–156.

10 S. Strbac, The effect of pH on oxygen and hydrogen peroxide reduction on polycrystalline Pt electrode, *Electrochim. Acta*, 2011, **56**, 1597–1604.

11 J. B. Goodenough and B. L. Cushing, in *Handbook of Fuel Cells—Fundamentals, Technology and Applications*, ed. W. Vielstich, H. A. Gasteiger and H. Yokokawa, Wiley, 2003, vol. 2, pp. 520–533.

12 J. Suntivich, H. A. Gasteiger, N. Yabuuchi, H. Nakanishi, J. B. Goodenough and Y. Shao-Horn, Design principles for oxygen-reduction activity on perovskite oxide catalysts for fuel cells and metal-air batteries, *Nat. Chem.*, 2011, **3**, 546–550.

13 Y. Wang and H. P. Cheng, Oxygen reduction activity on perovskite oxide surfaces: a comparative first-principles study of $LaMnO_3$, $LaFeO_3$ and $LaCrO_3$, *J. Phys. Chem. C*, 2013, **117**, 2106–2112.

14 J. O'M. Bockris and T. Otagawa, Mechanism of Oxygen Evolution on Perovskites, *J. Phys. Chem.*, 1983, **87**, 2960–2971.

15 D. Cao, L. Sun, G. Wang, Y. Lv and M. Zhang, Kinetics of hydrogen peroxide electroreduction on Pd nanoparticles in acidic medium, *J. Electroanal. Chem.*, 2008, **621**, 31–37.